Modelling of cohesion and adhesion damage of seal based on dynamic shear rheometer testing

Estimé Mambula Mukandila[a,*], Wynand Jacobus van der Merwe Steyn[b] and Terence Ian Milne[c]

[a]WorleyParsons RSA (Pty) Ltd, Pretoria, South Africa;

[b]Department of Civil Engineering, University of Pretoria, Pretoria, South Africa;

[c]Aurecon Centre, Tshwane, South Africa

*CONTACT Estimé Mambula Mukandila, estime.mukandila@worleyparsons.com

Abstract

Most current seal designs are based on the volumetric properties of materials and voids. In order to improve seal design, the possibility of introducing mechanistic principles into seal design was investigated. Introducing mechanistic concepts into seal design means that principles such as elasticity and viscoelasticity could be used in terms of stress-strain to explain phenomena such as damage in the seal structure. Two main failure parameters of seals – cohesion failure (fatigue cracking due to ageing of binder and loss of elasticity) and adhesion failure or stripping (occurring between stone to bitumen or bitumen to base) – are investigated using the complex modulus (G^*) which is one of the viscoelastic parameters of bituminous materials. This paper therefore investigates the testing procedure of cohesion fatigue damage (CFD) and Adhesion Fatigue Damage (AFD) of bituminous seal material using the Dynamic Shear Rheometer (DSR). The CFD and AFD modelling are based on the stiffness reduction principle of materials under the action of cyclic stress. Based on the Lifetime Optimisation Tool (LOT) research programme from Delft University of Technology, a DSR testing procedure and approach was adopted for seals. The tests were performed on 70/100 penetration grade bitumen columns (for CFD) and on stone columns constituted with dolorite glued together with 70/100 penetration grade bitumen (for AFD). It was observed that the model for CFD depends more on stress, while the model for AFD appears to depend more on temperature. This observation agrees with the fact that adhesion damage is more sensitive to temperature change, whereas cohesion damage is more prone to be influenced by applied fatigue stress. The CFD and AFD models provide an indication of non-linear development of the accumulated fatigue damage of seal. This is represented by the modelling of the change of G^*, as suggested in this investigation.

Keywords: Cohesion; adhesion; seal; DSR; damage; complex moduls; model

1. Introduction

Most current seal designs are based on the volumetric properties of materials and voids. In order to improve seal design, the possibility of introducing mechanistic principles into seal design was investigated, in South Africa (Milne 2004) and elsewhere in the world (Huurman 2010; Kathirgamanathan and Herrington 2014). Introducing mechanistic concepts into seal design meant that principles such as elasticity and viscoelasticity could be used in terms of stress-strain to explain phenomena such as damage in the seal structure. Viscoelastic parameters of bituminous materials such as the complex modulus (G^*) and phase angle (δ) are key elements in the understanding of performance, damage and failure of seal bituminous materials. Two main failure parameters of seals are the cohesion failure (fatigue cracking due to ageing of binder and loss of elasticity) and the adhesion failure or stripping (occurring between stone and bitumen or bitumen and base).

This paper investigates the testing procedure of cohesion fatigue damage (CFD) and Adhesion Fatigue Damage (AFD) of bituminous seal material using the Dynamic Shear Rheometer (DSR). The modelling of CFD and AFD evolution over the life of the seal based on test results is presented. The CFD and AFD investigations are based on the stiffness reduction principle of materials under the action of cyclic stress. The study was based on the original Lifetime Optimisation Tool (LOT) research programme from the Delft University of Technology in Netherlands (Huurman 2007).

The Asphalt Institute (1997) reported that the ideal testing equipment for addressing both the loading time and temperature behaviour dependency of bituminous binders is the DSR. The DSR is adapted for use with bitumen binder to evaluate both time and temperature effects. When used to test bitumen binders, the DSR measures the rheological properties such as the complex shear modulus (G^*) and phase angle (δ).

The basic DSR operation consists of placing bitumen between two parallel plates, one that is fixed (stator) and the other oscillating (rotor) (Figure 1). The stator and the rotor are also called the 'measuring system' or 'geometry'. Testing is performed by oscillating the spindle around its own axis point 'O' such that a radial line through point 'A' moves to point 'B', then reverses direction and moves through point 'A' to point 'C', followed by moving

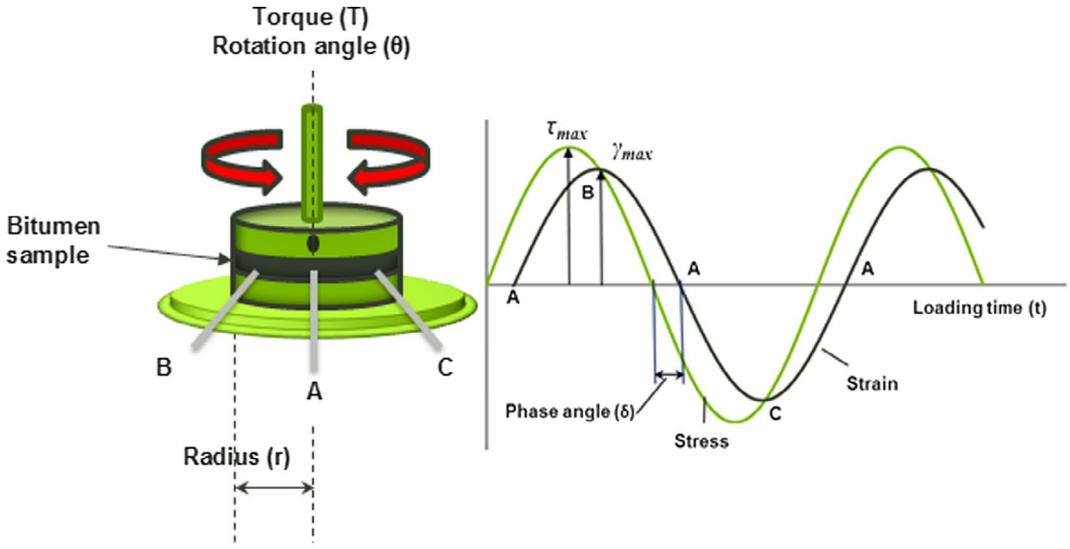

Figure 1. Schematic representation of DSR operation (Asphalt Institute 1997).

back from point 'C' to point 'A' (Figure 1). The responding strain/stress measurement is determined by applying a torque to a puck-shaped bituminous specimen, in response to the applied stress/strain (Liao 2007; Airey 1997). The angle formed by the lines AOB (or AOC) during the oscillating movement is called the deflection angle.

The latest DSR models are capable of handling a range of measuring systems. Common types of measuring systems are parallel plate, cone and plate, concentric cylinders (single or double gap), and solid torsional bar fixture. For a specific test and /or sample, the geometry can be chosen to provide the optimum working ranges of strain or strain rate, and stress (Anton Paar 2015; TA Instruments 2006).

The bitumen frequency response test is a standard DSR test as described in standards such as AASHTO (2005). This test often uses the parallel plate configuration as depicted in Figure 2. The purpose of this test is to provide viscoelastic response parameters such as G^* and δ at different temperatures and frequencies. The test is generally performed as strain controlled, in sweep frequency mode. The diameter and the gap between plates depend on the testing temperature.

2. Development of testing procedures for cohesion and adhesion fatigue damage

The performance prediction for road seals can be evaluated through the investigation of seal failure parameters. These failure parameters include:

- cracking due to low temperature and ageing of binder, which is referred to as cohesion failure within the binder, and
- adhesion failure or stripping, which occurs between the seal stone and binder.

The DSR was utilised as a testing device in the investigation of CFD (fatigue damage within the seal binder) and AFD (fatigue damage between seal stone and binder). The outcome of these tests was fatigue damage expressed in terms of stiffness (G^*) reduction as reported by Domone and Illstone (2010) and Sybilski *et al.* (2013). In the fatigue test the time sweep test was used instead of the standard frequency sweep test.

Special testing set-ups were required in order to perform cohesion and adhesion tests using the DSR. These testing set-ups were based on LOT research programme (Huurman 2007) (Figures 4 and 5).

The CFD test was performed using a bitumen column 6 mm in diameter and 20 mm high, fitted with stainless steel rings 8 mm in diameter and 4 mm high at each end. A clamping system was mounted to the DSR to hold the two ends of the bitumen column via the stainless rings. The test was performed in time sweep regime (Figure 3).

The AFD tests were performed using stone columns 10.9 mm in diameter and 15 mm high, glued together by a bitumen film of not more than 100 μm. A clamping system was mounted to the DSR to hold the two ends of the bitumen column (Figure 3).

Cohesion and adhesion testing protocols were developed based on the previous tests done at TU Delft (Khedoe and Moraal 2007).

The DSR test equipment is still in a development phase when used for the evaluation for seal design and performance. A number of issues were identified, and in Table 1 the various challenges faced in the development of the test protocol are summarised as proposed. A more detailed motivation and description is proposed in Mukandila (2016) (Tables 2 and 3).

3. Accumulated fatigue damage model of cohesion and adhesion

3.1. Principle of accumulated damage

Theyse and Van As (2010) reported that the current pavement design method used in South Africa estimates the structural capacity of a pavement from a condition of no distress to a condition of terminal distress, where terminal distress represents the level of distress for which the transfer functions were calibrated. No statement is made on how the terminal condition will be reached, but the classical methods estimate the number of axle loads that will result in the terminal condition. At best, a linear path can be assumed from zero distress to terminal distress.

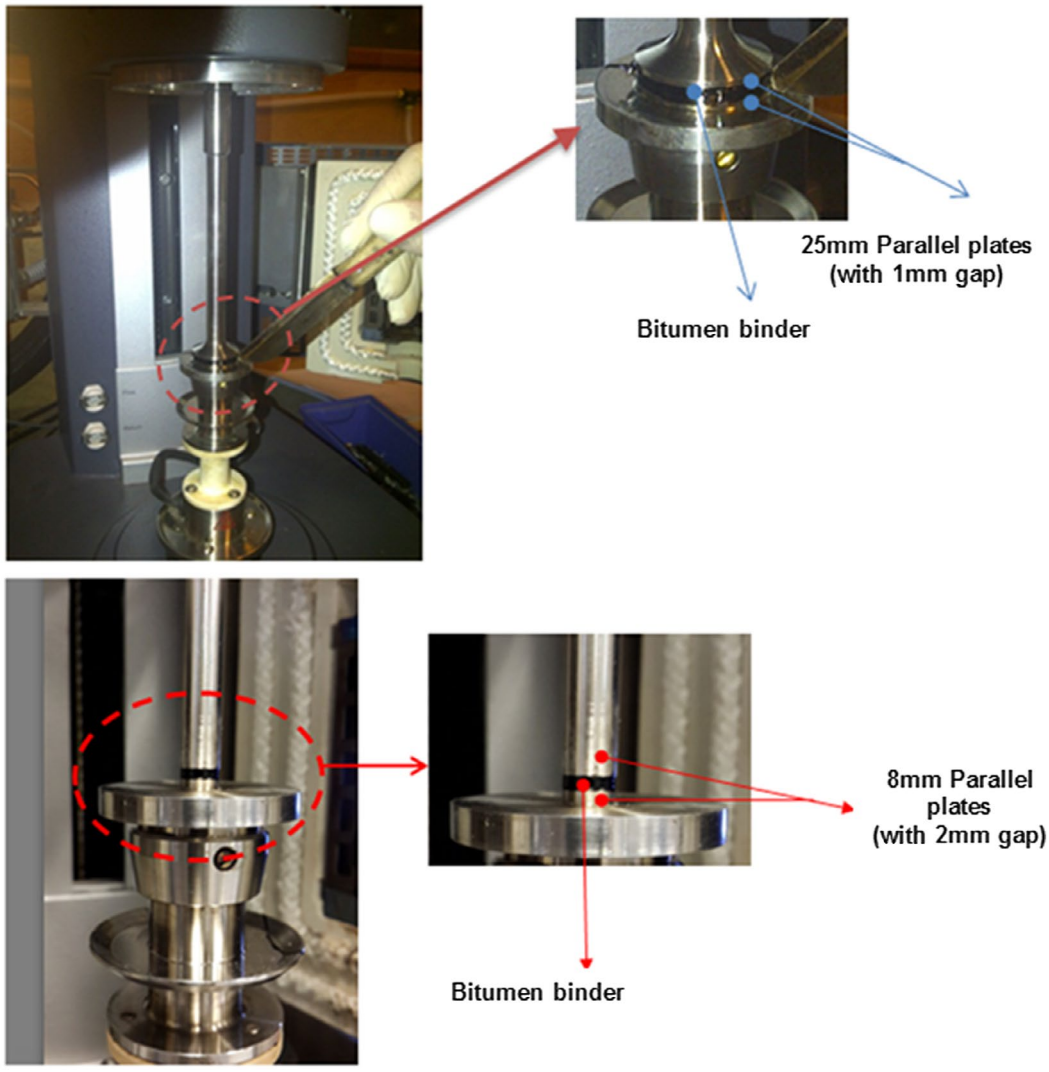

Figure 2. DSR parallel plate configuration.

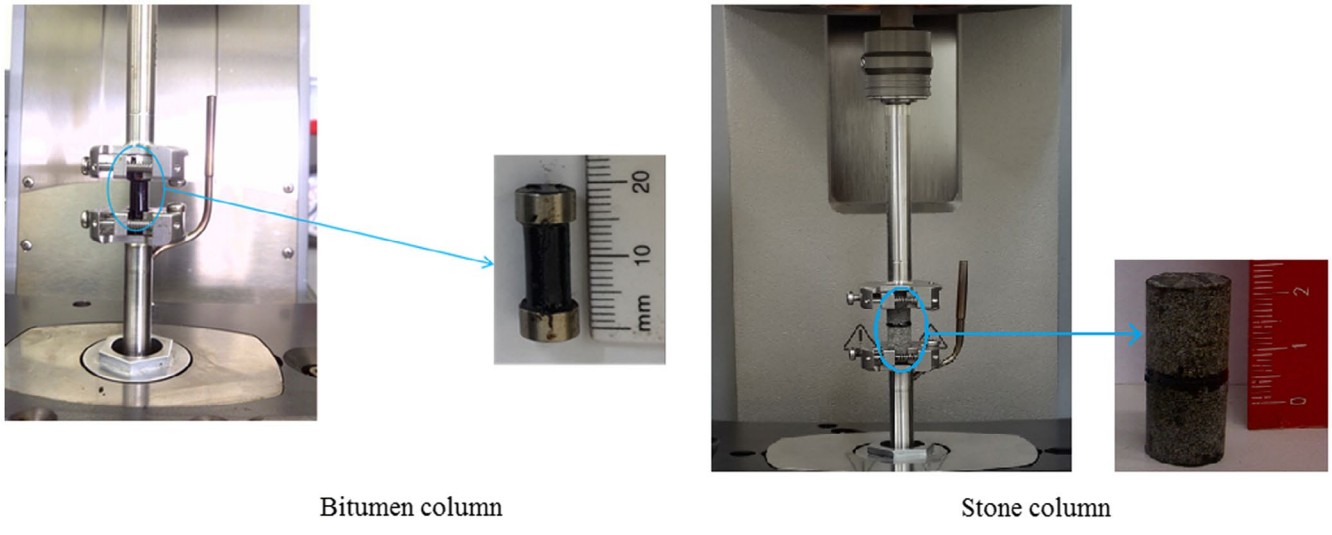

Figure 3. Bitumen column configuration for the DSR CFD test and Stone column configuration for the DSR AFD test.

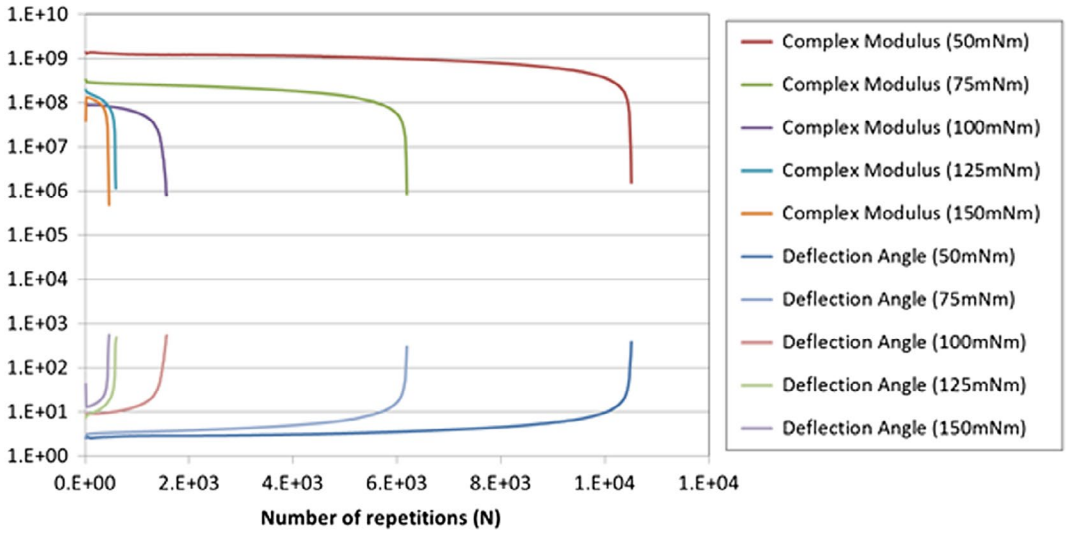

Figure 4. Complex modulus and deflection angle vs. time in stress-controlled mode at different temperatures for adhesion.

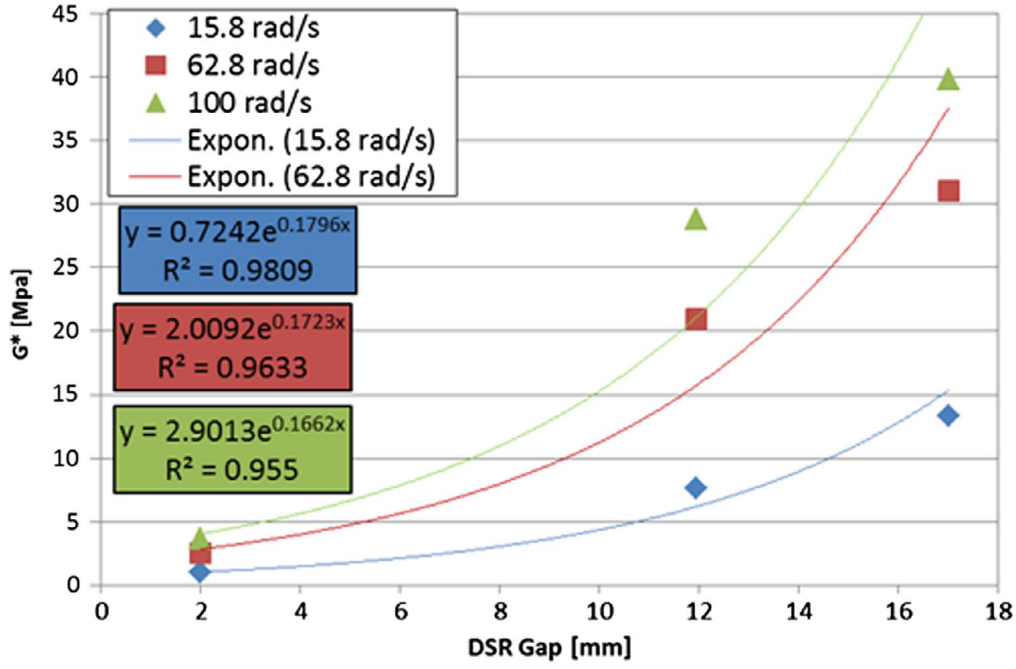

Figure 5. Complex modulus–DSR gap relationship.

Some of the more modern Mechanistic-Empirical (ME) pavement design methods use recursive simulation to simulate different periods of distress during the life cycle of the pavement. The outcome from these methods is therefore not a linear progression of distress, but an incremental increase in distress until an unacceptable level of distress is reached.

This concept can be elaborated on by modelling the development of the distress or the damage during the life of the pavement material. In this regard, it was decided to model CFD and AFD as evolutions of the damage with time; this was called the 'accumulated damage'. The damage is expressed by Equation (1).

$$D = 1 - \frac{G_N^*}{G_0^*} \quad (1)$$

where, N is a given the number of load repetitions, D is the fatigue damage after N repetitions, G_N^* is the complex modulus after N repetitions, and G_0^* is the initial complex modulus.

At the beginning of the test (no damage condition), $G_N^* = G_0^*$, from Equation (1), $D = 0$. When failure occurs in the sample, the stiffness of the material at the failure position reduces significantly and the ratio $\frac{G^*N}{G^*o}$ tends to zero. Thus, from Equation (1), D trends to 1 ($D \approx 1$). It can be concluded that, theoretically, the damage is expressed as a number between 0 and 1, with:

- 0 representing the no-damage condition (material having its initial dynamic shear modulus), and
- 1 representing failure condition.

Table 1. Challenges addressed with the test protocol (Mukandila 2016).

Challenge identified	Solution proposed
Stabilisation of the testing temperature in the chamber	The clamping system used induced testing temperature instability in the temperature test chamber fitted to the DRS. It is recommended that the clamping system is connected to the DSR operating system and this link is maintained
Choice of testing parameters, such as testing temperature, testing frequency, torque level, strain level, maximum testing time, etc	All these parameters were investigated in more detail (Mukandila, 2016) and the summary recommendation is shown in Table 2
Choice of testing mode between strain-controlled and stress-controlled mode (Monismith and Deacon, 1969)	DSR strain-controlled results show inconsistency. In Figure 4 the consistency with stress-controlled testing is demonstrated. Stress-controlled mode better reflects the interaction between a pavement and external forces and therefore stress-controlled testing was preferred
Impact of configuration changes of the DSR geometry on the test output (e.g. changing from parallel plate configuration to stone column configuration)	A variety of tests were conducted to determine this impact. Typically it was found the relationship between complex modulus and gap size could be expressed as an exponential function. Table 3 and Figure 5 represent this relationship. It should also be noted that sample diameter (which was not considered in the relationship) could affect the complex modulus results. Further research is needed
Comparison between tests done in pure shear mode and tests done in combined shear and normal stress mode	Normal DSR tests induce only pure shear stress. A trial was conducted during DSR testing which would incorporate the limited normal force provided by the DSR. The tests performed under compression did not display a specific failure time. This complex behaviour might be due to the counter-effect of compression on the fracture phenomenon (compression force tends to mitigate the fracture of the material). The inclusion of normal force during tests with the currently available DSR was not yet been mastered. Thus, focus was placed only on tests performed under pure shear
Influence of the binder film thickness between stones (in the AFD test) on the mode of failure (AFD failure or CFD failure)	Film thickness was arbitrarily set to 100 µm (previously 15 µm) used for the stone column to relate better with actual seal stone film thickness. The greater film thickness increased the probability of cohesion failure instead of adhesion failure. To confirm adhesion failure, the samples were visually inspected after the tests
Verification of testing repeatability	Tests were performed in different laboratories using different models of the DSR equipment from different manufacturers. Repeatability was assessed by comparing the results of similar samples using different DSR systems, and by comparing the results of similar samples from tests repeated on the same DSR. The comparison based on different DSR systems was performed on the frequency sweep test. Correlations found were good and repeatability of tests were also found to be acceptable
It appears that fatigue damage during the time sweep test could be due to the combined effect of the viscoelastic properties of a material and a change in the radius of the sample	To account for the sample's radius change (Hintz and Bahia, 2013), it is suggested to monitor the rate of crack progression in the evaluation of the fatigue damage. Due to the anticipated complexity of a crack progression study, this investigation assumed that the fatigue damage is due only to the viscoelastic properties of the material
The parallel plate configuration was used for the CFD tests. Compared with the bitumen column, poor response of the parallel plates was noticed, especially at low temperatures (0–10 °C). De-bonding was observed	A possible solution to address this issue is to manufacture parallel plates with rough surfaces to resist the de-bonding effect

Table 2. Testing parameters for CFD and AFD.

Test type	Strain [%]	Torque [mNm]	Frequency [rad/s]	Max time [hours]	Temperature [°C]
CFD	2	1 to 50	62.8	2	0; 5; 10; 15; 20; 23; 25
AFD	2	50 to 200	62.8	2	10; 20; 23; 25

Table 3. Data for complex modulus – DSR–gap relationship.

		70/100 using parallel plate from DELFT	70/100 using 6 mm stone column from DELFT	70/100 using 10.9 mm stone column from SRT/ South Africa
			G^* [MPa]	
	Gap [mm]	1	11.93	17
Frequency [rad/s]	at 15.8 rad/s	0.964	7.67	13.3
	at 62.8 rad/s	2.57E+06	21.0	31.0
	at 100 rad/s	3.64	28.8E+07	39.8

3.2. Model development

The fatigue damage model of cohesion and adhesion are based on DSR test results performed on 70/100 penetration grade bitumen columns (for CFD) and stone columns constituted with dolorite glued together with 70/100 penetration grade bitumen (for AFD) (Mukandila 2016).

The accumulated damage model is developed using the 'sudden drop' principle. The model is developed using the criteria of a 'sudden drop' in the G^* and the deflection angle (θ). The sudden drop of G^* fixes the maximum damage to a value closer to one. The aim is to model the development of the damage during the seal's life from a state of no damage (damage = 0) to the failure state (damage ≈1). The development of the accumulated damage model was based on the establishment of the fatigue damage (D) as a function of the number of repetitions (N), stress (τ) and temperature (T). Expressing the model in terms of stress and temperature accounted, respectively, for the traffic and the environmental effect. The stress used in this case was a shear stress derived from torque level obtained from DSR measuring as presented in Equation (2).

$$\tau = K\frac{2M}{\pi r^3} \tag{2}$$

where, τ is the shear stress [Pa], M is the torque [mNm], r is the radius of the test sample; r = 3 mm for the bitumen column and

r = 5.45 mm for the stone column, K is the conversion factor; K = 1.00E+6.

For simplification reasons, the modelling was expressed in terms of the normalised number of repetitions (N_n), instead of the actual number of repetitions (N). The normalised number of repetitions (N_n) is presented in Equation (3). N_n also varies from zero to one.

$$N_n = \frac{N}{N_F} \tag{3}$$

where N_n is the normalised number of repetitions, N is the number of repetitions at a given time, and N_F is the number of repetitions to failure.

The development of the accumulated modelling of CFD and AFD was done in two steps. In the initial step the damage at different torque levels for each separate temperature was modelled, and thereafter there was a generalised step in which all the models constructed at each temperature (isotherms) were combined into one global model. The global modelling consisted of adjustment of the model coefficients of the initial models.

The accumulated damage models of CFD and AFD were developed in the following steps to produce the final model:

(1) The record of the variation of G^* with the number of repetitions (N) collected at different torque (stress) levels for a given temperature constitutes the major DSR testing outcome used in this modelling. Using the sudden drop principle, the complex modulus at failure $\left(G^*_{N_f}\right)$ was determined for each stress level at a given temperature of the CFD and AFD tests.

(2) The calculations of damage from the DSR results (D_X-calc) for CFD and AFD of each repetition were processed using Equation (1). The damage varied from zero (no damage) to one (failure state). In the symbol 'D_X-calc', the subscript $X = C$ in the case of CFD and $X = A$ in the case of AFD.

(3) Using Equation (3), the number of repetitions was normalised to range from zero to one.

(4) The damage (D_X-calc) was expressed as a function of the normalised number of repetitions (N_n), $D_X = f(N_n)$, for each torque level for a given temperature. It was found that a rational function called the 'Nelder' function provided the better fit for each stress level for a given temperature. This function is presented in Equation (4). The Nelder function fitted both the CFD and AFD models well.

$$D_X = \frac{N_n + a_X}{b_X + c_X(N_n + a_X) + w_X(N_n + a_X)^2} \tag{4}$$

where, D_X is the fatigue damage, N_n is the number of load repetitions, a_X, b_X, c_X and w_X are the model coefficients or Nelder coefficients, and X = C in the case of CFD and $X = A$ in the case of AFD.

(5) In the initial stage of model development, Equation (4) was rewritten as expressed in Equation (5). The initial values of the Nelder coefficients (a'_X, b'_X, c'_X and w'_X) for each stress level for a given temperature were determined by a regression analysis. In the regression analysis, the modelled damage was fitted to the calculated damage from measured data by minimising the error between the two damages. Typical graphs of damage as a function of the normalised number of repetitions are presented in Figure 6. Examples of initial Nelder coefficients, in the case of CFD and AFD tested at 25 °C and at different stress levels, respectively, presented in Tables 4 and 5.

$$D'_X = \frac{N_n + a'_X}{b'_X + c'_X(N_n + a'_X) + w'_X(N_n + a'_X)^2} \tag{5}$$

where, D'_X is the initial value of the fatigue damage, N_n is the number of load repetitions, a'_X, b'_X, c'_X and w'_X are the initial values of the model coefficients (or Nelder coefficients) determined at each torque level of each testing temperature of CFD and AFD.

(6) A relationship between each initial value of the Nelder coefficient and the torque (stress) level could be observed at each temperature for both CFD and AFD. The relationship was developed by selecting an appropriate fitting function. These relationships for a'_X, b'_X, c'_X and w'_X are presented in Equations (6)–(9), respectively. Examples of graphs presenting the development of these equations are illustrated in Figures 7 and 8, respectively, for CFD and AFD.

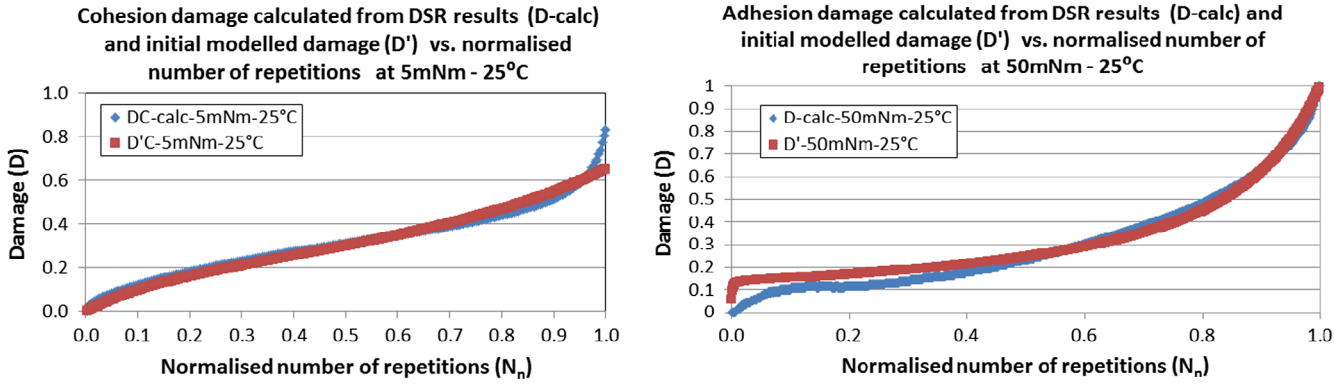

Figure 6. Damage calculated from DSR results (D_C-calc) and initial modelled damage (D'_C) vs. normalised number of repetitions for cohesion at 5 m Nm – 25 °C and adhesion at 50 m Nm – 25 °C.

Table 4. Initial values of Nelder coefficients in the case of cohesion within 70/100 bitumen at 25 °C and at different stress levels.

τ [Pa]	a'_C (25 °C)	b'_C (25 °C)	c'_C (25 °C)	w'_C (25 °C)
1.19E+05	−0.003	0.750	2.859	−2.082
2.39E+05	−0.044	0.811	1.445	−0.825
3.58E+05	−0.111	0.950	0.863	−0.121
4.77E+05	−0.200	1.150	−0.029	1.366
5.97E+05	−0.270	1.400	−2.308	2.324

Table 5. Initial values of Nelder coefficients in the case of adhesion between dolor-ite and 70/100 bitumen at 25 °C and at different stress levels.

τ [Pa]	a'_A (25 °C)	b'_A (25 °C)	c'_A (25 °C)	w'_A (25 °C)
1.98E+05	−0.001	0.005	7.115	−6.129
2.96E+05	−0.002	0.008	5.885	−4.947
3.95E+05	−0.005	0.013	4.591	−3.625
4.94E+05	−0.008	0.027	4.008	−3.077

$$a'_X = \alpha'_{X1}\tau + \alpha'_{X2} \tag{6}$$

$$b'_X = \beta'_{X1}e^{\beta'_{X_2}}\tau \tag{7}$$

$$c'_X = \gamma'_{X1}\tau + \gamma'_{X2} \tag{8}$$

$$w'_X = \omega'_{X1}\tau + \omega'_{X2} \tag{9}$$

where, a'_X, b'_X, c'_X and w'_X are the initial Nelder coefficients for CFD and AFD, $a'_{X1}, a'_{X2}, \beta'_{X1}, \beta'_{X2}, \gamma'_{X1}, \gamma'_{X2}, \omega'_{X1}$ and ω'_{X2} are the global model coefficients (global coefficients). These global model coefficients are determined for each testing temperature of CFD and AFD. τ is the shear stress level calculated from the torque level using Equation (2) As an example of using the subscript X in the case of CFD, Equation (7) would be written as presented in Equation (10).

$$b'_C = \beta'_{C1}e^{\beta'_{C2}}\tau \tag{10}$$

The values of the global coefficients are presented in Table 6 in the case of CFD and in Table 7 in the case of AFD.

(7) As discussed in the introduction to this section, the ultimate aim of the accumulated modelling was to attempt to express the damage as a function of stress and temperature. Equations (6)–(9) represented functions that connect the initial Nelder coefficients to the stress levels at each tested temperature. The combination of each initial Nelder coefficient in one graph (as presented in Figure 9 for b'_C) allowed the assessment of a possible relationship linking the initial values of the Nelder coefficient to the temperature.

The investigation of this relationship was based on the global model coefficients. In some cases, it was found that the global model coefficients could be expressed as a function of the stress level or of the temperature or of both of them. In the specific case of initial Nelder coefficient b'_C as expressed by Equation (10), it was observed that the global model coefficient β'_{C1} could be expressed as a linear function of temperature. This is presented in Figure 10 and expressed by Equation (11). No obvious relationship was found for β'_{C2} – neither with stress level, nor with temperature; thus β'_{C2} could be expressed as a constant.

$$\beta'_{C1} = \beta_{C1}T + \beta_{C2} \tag{11}$$

where, β'_{C1} is the global model coefficient, β'_{C1} and β_{C2} are constants in the model.

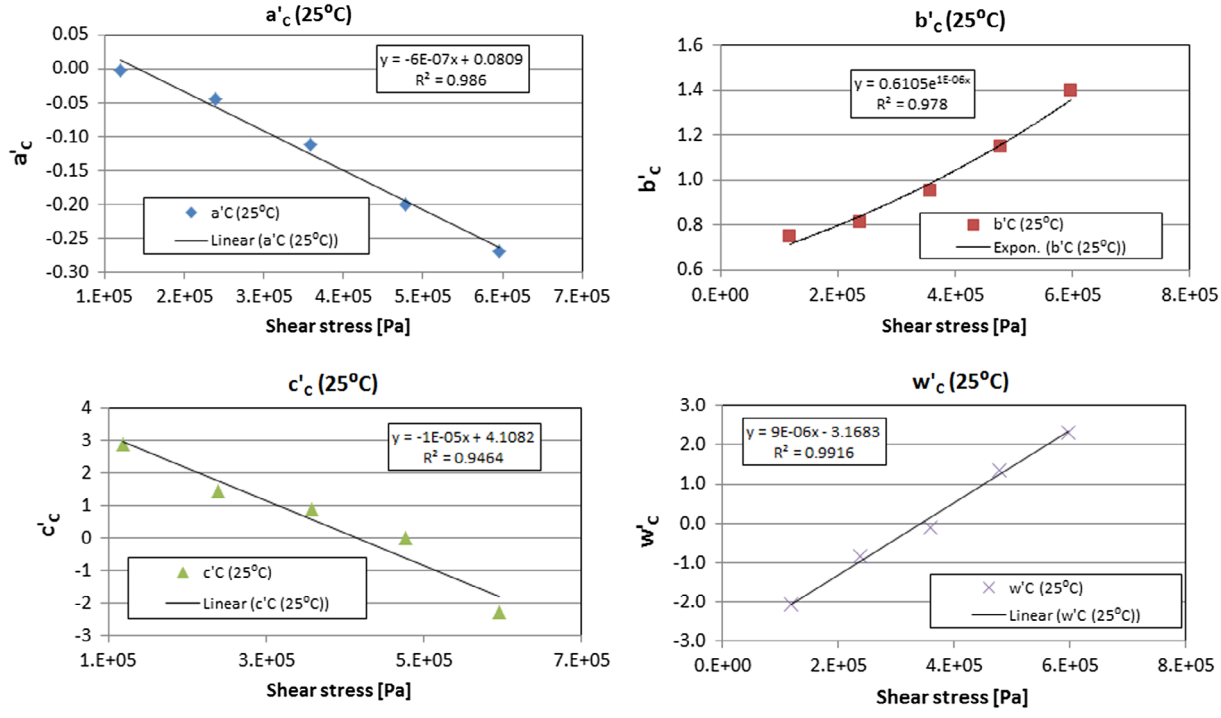

Figure 7. Graphic development of relationship between the initial Nelder coefficients and stress level for CFD at 25 °C.

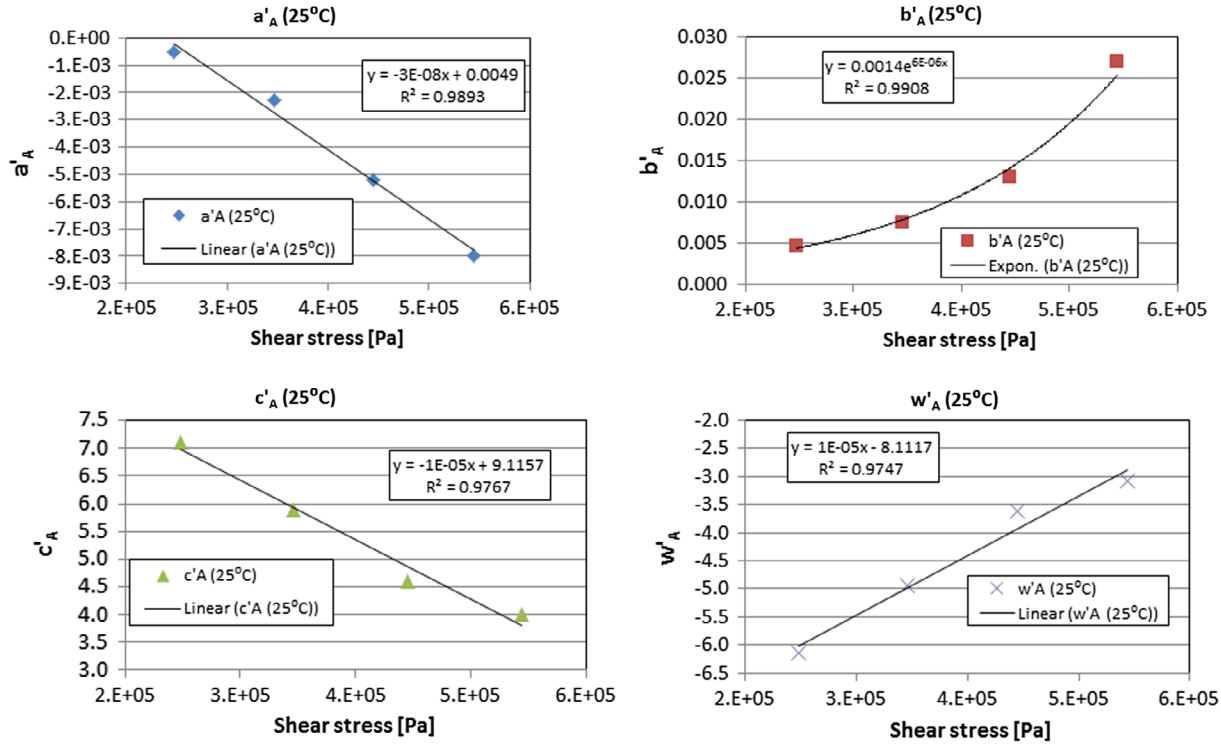

Figure 8. Graphic development of relationship between the initial Nelder coefficients and stress level for AFD at 25 °C.

Table 6. Values of global coefficients for CFD.

Initial Nelder coefficients for CFD	Temperature [°C]						
	0	5	10	15	20	23	25
α'_{C1}	−1.53E−08	−2.57E−09	−1.89E−08	−7.55E−08	−1.61E−07	−5.17E−07	−1.38E−02
α'_{C2}	1.1E−02	4.4E−04	3.6E−03	9.6E−03	2.28E−02	8.20E−02	8.09E−02
β'_{C1}	1.39E−03	1.00E−01	2.25E−01	3.40E−01	4.89E−01	5.74E−01	6.11E−01
β'_{C2}	5.98E−06	2.70E−06	2.10E−06	2.00E−06	1.40E−06	1.34E−06	1.34E−06
γ'_{C1}	−1.41E−05	−2.13E−06	−3.72E−06	−5.54E−06	−5.97E−06	−9.05E−06	−9.90E−06
γ'_{C2}	1.63E+01	4.17E+00	3.71E+00	3.87E+00	3.66E+00	3.65E+00	4.11E+00
ω'_{C1}	8.48E−06	2.80E−06	2.05E−06	4.49E−06	3.97E−06	7.40E−06	9.22E−06
ω'_{C2}	−1.02E+01	−4.09E+00	−2.30E+00	−2.89E+00	−2.42E+00	−2.63E+00	−3.17E+00

Table 7. Values of global coefficients for AFD.

Initial Nelder coefficients for AFD	Temperature [°C]			
	10	20	23	25
α'_{A1}	−9.61E−09	−4.90E−08	−2.51E−08	−2.56E−08
α'_{A2}	5.70E−02	2.37E−02	8.23E−03	4.86E−03
β'_{A1}	4.23E+00	2.40E−01	2.87E−03	1.36E−03
β'_{A2}	5.2E−07	4.3E−06	5.2E−06	5.91E−06
γ'_{A1}	−0.0002	−1.36E−05	−7.02E−06	−1.07E−05
γ'_{A2}	117.18	7.81	7.27	9.12
ω'_{A1}	2.09E+00	7.20E−06	7.06E−06	1.06E−05
ω'_{A2}	5.35153	5.77	−6.21	−8.11

Table 8 provides information on all global model coefficients in terms of their relationship with stress level and/or temperature. This information was based on the observed trends of the global model coefficients as a function of stress level and/or temperature. Details on this information are presented in Mukandila (2016).

By substituting Equation (11) in Equation (10), the adjusted model coefficient is obtained as represented in Equation (12). The adjusted model coefficient then replaces the initial Nelder coefficients.

$$b_C = (\beta_{C1} T + \beta_{C2}) e^{\beta_{C3} \tau} \tag{12}$$

where, b_c is an adjusted model coefficient for CFD, β_{C1}, β_{C2} and β_{C3} are model constants for CFD, (It should be noted that $\beta_{C3} = \beta'_{C2}$ with β'_{C2} as presented in Equation (10)), T is the temperature, τ is the shear stress.

Other adjusted model coefficients and global model coefficients were obtained in a similar manner and are presented in Equations (13)–(19).

$$a_C = \alpha_{C1} \tau + \alpha_{C2} \tag{13}$$

$$c_C = \gamma_{C1} \tau + \gamma_{C2} \tag{14}$$

$$w_C = \omega_{C1} \tau + \omega_{C2} \tag{15}$$

$$a_A = \alpha_{A1} \tau + \alpha_{A2} T + \alpha_{A3} \tag{16}$$

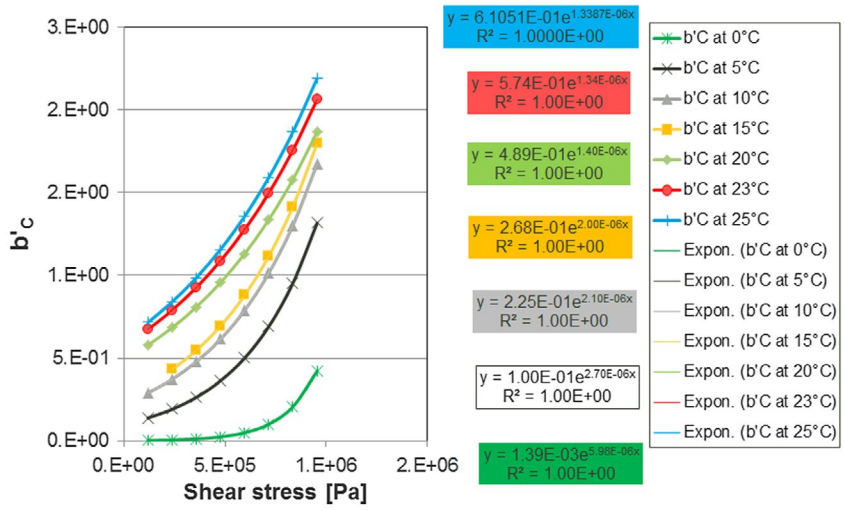

Figure 9. Combination of all Nelder coefficients b'_C on a unique graph.

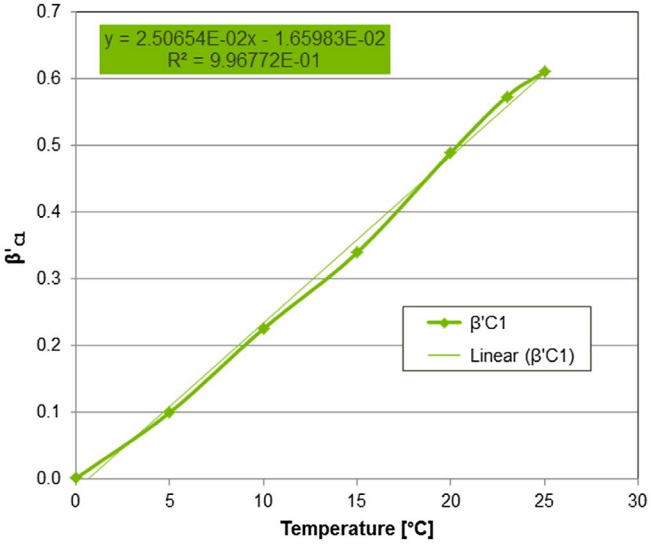

Figure 10. Relationship between β'_{C1} and temperature.

Table 8. Information on the relationship between global model coefficients and stress level and/or temperature, based on observed trends.

Global model coefficients	Relationship with τ	Relationship with T	Observation
a'_{C1}	No	No	a'_{C1} = Constant
a'_{C2}	No	No	a'_{C2} = Constant
β'_{C1}	Yes	Yes	$\beta'_{C1} = f(\tau, T)$
β'_{C2}	No	No	β'_{C2} = Constant
γ'_{C1}	No	No	γ'_{C1} = Constant
γ'_{C2}	No	No	γ'_{C2} = Constant
ω'_{C1}	No	No	γ'_{C1} = Constant
ω'_{C2}	No	No	γ'_{C2} = Constant
a'_{A1}	Yes	Yes	$\alpha'_{A1} = f(\tau, T)$
a'_{A2}	No	No	α'_{A2} = Constant
β'_{A1}	No	No	β'_{A1} = Constant
β'_{A2}	Yes	Yes	$\beta'_{A2} = f(\tau, T)$
γ'_{A1}	No	No	γ'_{A1} = Constant
γ'_{A2}	No	No	γ'_{A2} = Constant
ω'_{A1}	No	No	ω'_{A1} = Constant
ω'_{A2}	No	No	ω'_{A2} = Constant

$$b_A = \beta_{A1} e^{(\beta_{A2} T + \beta_{A3})\tau} \quad (17)$$

$$c_A = \gamma_{A1} T + \gamma_{A2} \quad (18)$$

$$w_A = \omega_{A1} T + \omega_{A2} \quad (19)$$

where, a_C, c_C, and w_C are the adjusted model coefficients for CFD, a_A, b_A, c_A and w_C are the adjusted model coefficients for AFD, a_{C1}, $a_{C2,}$ γ_{C1}, γ_{C2}, ω_{C1} and ω_{C2} are model constants for CFD, α_{A1}, α_{A2}, α_{A3}, β_{A1}, β_{A2}, β_{A3}, γ_{A1}, γ_{A1}, ω_{A1} and ω_{A2} are model constants for AFD, T is the temperature, and τ is the shear stress.

(8) The initial CFD and AFD models developed at each stress level and each temperature were generalised based on adjusted values of the model coefficients (a_X, b_X, c_X and w_X). The adjusted values of the model coefficients were included in Equation (4) to form the global damaged model at each level for each specific temperature. A typical plot of this global damage model for CFD in the case of the 70/100 bitumen modelled at the temperature of 25 °C is presented in Figure 11.

The global damage model was generalised to include all temperatures and was symbolised by 'D_X-model'. D_X-model in the case of CFD is symbolised by D_C and D_X-model in the case of AFD is symbolised by D_A. These two models are respectively referred to as the CFD model within the seal's bitumen and the AFD between seal stone and bitumen. The CFD model within the seal's bitumen is presented in Equation (20). Similarly, the adhesion between seal stone and bitumen is presented in Equation (21). These two models are presented graphically in Figure 12.

$$D_C = \frac{N_n + a_C}{b_C + c_C(N_n + a_C) + w_C(N_n + a_C)^2} \quad (20)$$

$$D_A = \frac{N_n + a_A}{b_A + c_A(N_n + a_A) + w_A(N_n + a_A)^2} \quad (21)$$

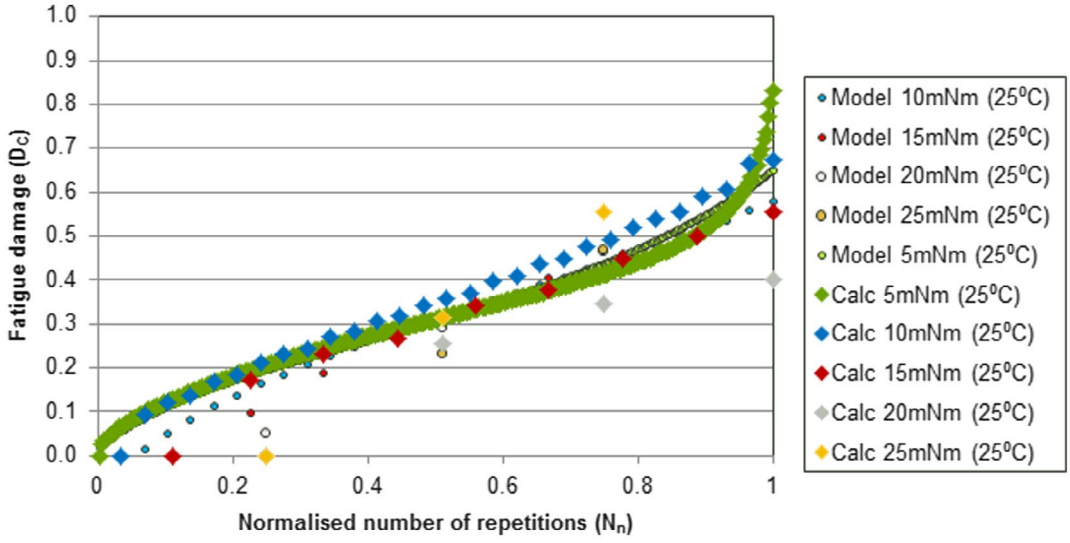

Figure 11. Plot of global damage model for CFD in the case of the 70/100 bitumen modelled at the temperature of 25 °C.

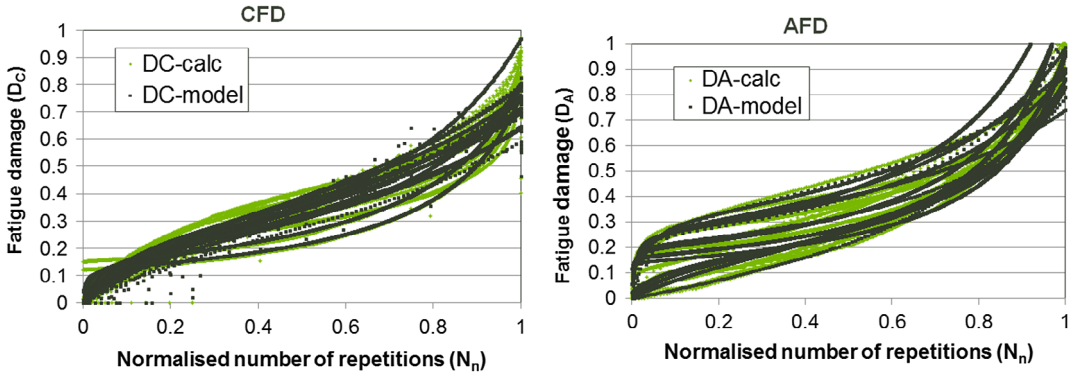

Figure 12. Normalised cohesion and AFD models during seal life.

In these two equations, the adjusted model coefficients are as presented in Equations (12)–(19). An example of the values of adjusted model coefficients in the case of CFD tested at 25 °C and at different stress levels is presented in Table 9.

The D_X-models (for CFD and AFD) were compared with the damage calculated (D_X-calc) from the DRS data. The coefficient of determination (R^2) and the Standard Error of Estimate (SEE) are presented in Table 10. In addition, the correlations between D_X-calc and D_X-model are given in Figure 13 for CFD and AFD. It can be concluded that there is an acceptable correlation between the damage calculated from laboratory data and from the model.

Table 9. Values of adjusted model coefficients in the case of CFD tested at 25 °C and at different stress levels.

τ [Pa]	a'_C (25 °C)	b'_C (25 °C)	c'_C (25 °C)	w'_C (25 °C)
1.193E+05	0.012	7.1567E−01	2.927	−2.068
2.386E+05	−0.057	8.3961E−01	1.747	−0.968
3.579E+05	−0.126	9.8500E−01	0.566	0.132
4.772E+05	−0.195	1.1556E+00	−0.615	1.233
5.965E+05	−0.264	1.3557E+00	−1.796	2.333

Table 10. Coefficient of determination and SEE for CFD and AFD.

	CFD	AFD
R^2	0.98	0.97
SEE	0.04	0.08

3.3. Model discussion

The development of the accumulated damage was based on the establishment of the fatigue damage as a function of number of repetitions, shear stress and temperature. In this process, the Nelder function was used as a model function for both CFD and AFD. The Nelder coefficients were used as initial model values. Possible relationships linking the Nelder coefficients to the shear stress and/or the temperature were investigated. In the case of confirmation, the relationships were expressed via the global model coefficients which were adjusted in the generalised and final CFD and AFD models.

Considering the adjusted coefficients as presented in Equations (12)–(19), it appears that the adjusted coefficients for CFD could be easily expressed as a function of the shear stress, while the adjusted coefficients for AFD tend to be expressed more easily as a function of temperature. It can thus be concluded

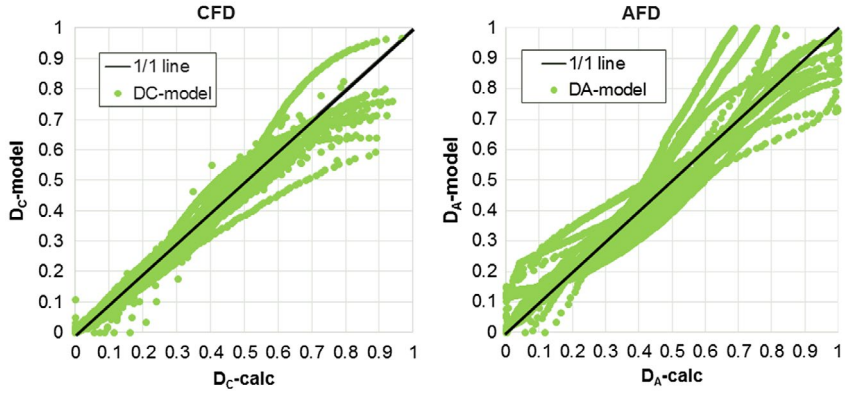

Figure 13. Correlation between damage calculated from laboratory data and modelled damage in the case of cohesion and AFD.

that the generalised model for CFD depends more on stress, whereas the generalised model for AFD appears to depend more on temperature. This observation seems to agree with the fact that adhesion damage is more sensitive to temperature change, while cohesion damage is more prone to be influenced by applied stress. As a result of this observation it is suggested that it be investigated whether the adhesion phenomenon could be considered as a 'non-fatigue' mechanism.

3.4. Contribution of the model to the mechanistic design of seal

Cohesion and adhesion are major factors in the damage and failure of the bitumen and bituminous seal. In this regard, the stiffness of the bitumen and bituminous seal materials within the binder, and between the stone and the binder, should be considered as essential inputs in the mechanistic analysis of seals.

The development of fatigue damage model was based on the stiffness of bituminous materials. In the case of dynamic shear loading, the stiffness of the bituminous materials is represented by the complex modulus and the phase angle. The complex modulus could be used as inputs in the mechanistic analysis of seals.

The 'accumulated fatigue damage' model could be motivated by the 'recursive simulation' models under development to be included in the SARDS. One of the ways used by SARDS to develop the recursive principle is the 'memory-less' concept. The memory-less concept introduced by Theyse and Van As (2010) is based on recent trends of mechanistic-empirical design method development towards modelling the incremental damage that occurs within recursive periods. Traffic loading, environmental conditions and pavement characteristics remain consistent within each recursive period but vary from one recursive period to the next. Given the changing conditions from one recursive increment to the next, the damage incurred in successive recursive increments is not the same. The total damage is accumulated by the addition of the incremental damage from each recursive increment. Mechanistic-empirical design methods based on this approach are referred to as 'recursive' mechanistic-empirical design methods. Theyse (2013) developed the memory-less principle (under the recursive simulation models) to predict the future damage and/or the failure of a material based only on the knowledge of current damage and the rate of the damage; therefore the damage history is not taken into account.

The implementation of the recursive simulation models requires knowledge of the modelling parameters (such as the stiffness) characterising the continuous damage during the life. The CFD and AFD models offer a practical advantage consisting of the possibility to be adapted and incorporated in the recursive simulation models as developed by SARDS. The CFD and AFD models provide an indication of non-linear development of the accumulated fatigue damage within bitumen and between bitumen and stone in the case of seal. This is represented by the modelling of the change of G^*, as suggested in this investigation.

4. Conclusion

The investigation of the cohesion and adhesion damage model of seals based on DSR testing requires the following:

- development of a testing procedure as cohesion and adhesion could not be accommodate by the standard parallel plate configuration of DSR, and
- development of CFD and AFD of bituminous seal material in line with the introduction of mechanistic design in the performance prediction of seal.

Based on the LOT research programme from TU Delft, a DSR testing procedure and approach was adopted for seal condition. The tests were performed on 70/100 penetration grade bitumen columns (for CFD) and stone column constituted with dolorite glued together with 70/100 penetration grade bitumen (for AFD). Results from the testing activities were analysed and modelled.

The aim of developing the accumulated damage model was to allow monitoring of the evolution of damage with time. This was based on the establishment of the fatigue damage as a function of the number of wheel load repetitions, shear stress and temperature. In this process, the Nelder function was used as a model function for both CFD and AFD. The Nelder coefficients were used as initial model coefficients values. Possible relationships linking the Nelder coefficients to the shear stress and/or the temperature were investigated. For model confirmation, the relationships were expressed via the global model coefficients, which were expressed as functions of shear stress and/or temperature. The global model coefficients were adjusted in the generalised and final CFD and AFD models. In this way the CFD

model within the seal's bitumen and AFD between seal stone and bitumen were obtained. It was observed that the generalised model for CFD depends more on stress, while the generalised model for AFD appears to depend more on temperature. This observation seems to agree with the fact that adhesion damage is more sensitive to temperature change, whereas cohesion damage is more prone to be influenced by applied fatigue stress.

Acknowledgment

Dr. Emile Horak is acknowledged for the review of the paper.

Disclosure statement

No potential conflict of interest was reported by the authors.

Funding

This work was supported by SANRAL.

References

Airey, G.D., 1997. *Rheological characteristics of polymer modified and aged bitumens*. Thesis (PhD). Department of Civil Engineering, University of Nottingham.

American Association of State Highway and Transportation Officials (AASHTO), 2005. *Determining the rheological properties of asphalt using a dynamic shear rheometer (DSR), AASHTO T 315-05*. Standard Method of test.

Anton Paar, 2015. *The modular compact rheometer series*. Catalogue, Graz.

Asphalt Institute, 1997. Performance-graded asphalt binder specification and testing. Superpave series no. 1 (SP-1). Lexington, KY.

Domone, P. and Illstone, J., eds., 2010. *Construction materials: their nature and behaviour*. 4th ed. London: Taylor & Francis.

Hintz, C. and Bahia, H., 2013. *Understanding mechanisms leading to asphalt binder fatigue in the dynamic shear rheometer (DSR), road materials and pavement design*. London. Taylor & Francis.

Huurman M., 2007. *Lifetime optimisation tool (LOT)*. Main report. Report 7-07-170-1. Technical University of Delft.

Huurman, M., 2010. Developments in 3D surfacing seals FE modelling. *International Journal of Pavement Engineering*, 11 (1), 1–12.

Kathirgamanathan, P. and Herrington, P.R., 2014. Numerical modelling of road with chip seal surfacing layer. *Proceeding of Jaffna University International Research Conference (JUICE 2014)*, 370–376.

Khedoe, R.N. and Moraal, J., 2007. *Sample preparation and laboratory testing for the LOT research program*. Report 7-07-170-4. Lifetime Optimisation Tool (LOT), Laboratory of Road and Railway Engineering, Delft University of Technology.

Liao, M.C., 2007. *Small and large strain rheological and fatigue characterisation of bitumen-filler mastics*. Thesis (PhD). University of Nottingham.

Liu, L., 2007, *Engineering properties of rocks, Rock Mechanics III*. Mansfield, CT. Lecture notes, Department of Civil and Environmental Engineering, University of Connecticut.

Milne, T.I., 2004. *Towards a performance-related seal design method for bitumen and modified road seal binders*. Thesis (PhD). University of Stellenbosch.

Monismith, C.L. and Deacon, J.A., 1969. Fatigue of asphalt paving mixtures. *ASCE Journal of the Transport Engineering Division*, 95, 154–161.

Mukandila E.M., 2016. *Investigation of rheological response, cohesion and adhesion fatigue damage of bituminous road seal materials* Unpublished thesis (PhD). Faculty of Engineering, University of Pretoria.

Sybilski, D., *et al.*, 2013. *Binder testing, advances in interlaboratory testing and evaluation of bituminous materials*, RILEM State-of-the-Art Report. Vol IX. Dordrecht: Springer.

TA Instruments, 2006, *AR-G2/AR 2000ex Operator's Manuel*. Revision C. New Castle.

Theyse, H.L., 2013. *Revision of the South African pavement design method* SANRAL/SAPDM/B-4/2013-03 Report. Pretoria: SANRAL.

Theyse, H.L. and Van As, C., 2010. *Stochastic recursive simulation, preliminary system design*. Version: 1st Draft, Draft Contract Report SANRAL-SAPDM-E3-2010-01, Revision of the South African Pavement Design Method. Pretoria: SANRAL.